Responding to the signal and the noise: behavior of planktonic gastropod larvae in turbulence

Michelle DiBenedetto[1,2,*,†], Karl R. Helfrich[1], Anthony Pires[3], Erik J. Anderson[4] and Lauren S. Mullineaux[2]

[1] Woods Hole Oceanographic Institution, Department of Physical Oceanography, Woods Hole, 02543, USA
[2] Woods Hole Oceanographic Institution, Department of Biology, Woods Hole, 02543, USA
[3] Dickinson College, Department of Biology, Carlisle, 17013, USA
[4] Grove City College, Department of Mechanical Engineering, Grove City, 16127, USA
[†] Present address: University of Washington, Department of Mechanical Engineering, Seattle, 98195, USA
*Author for correspondence: mdiben@uw.edu

Abstract

Swimming organisms may actively adjust their behavior in response to the flow around them. Ocean flows are typically turbulent, and characterized by chaotic velocity fluctuations. While some studies have observed planktonic larvae altering their behavior in response to turbulence, it is not always clear whether a plankter is responding to an individual turbulent fluctuation or to the time-averaged flow. To distinguish between these two paradigms, we conducted laboratory experiments with larvae in turbulence. We observed veliger larvae of the gastropod *Crepidula fornicata* in a jet-stirred turbulence tank while simultaneously measuring two-components of the fluid and larval velocity. Larvae were studied at two different stages of development, early-stage and late-stage, and their behavior was analyzed in response to different characteristics of turbulence: acceleration, dissipation, and vorticity. Our analysis considered both the effects of the time-averaged flow and the instantaneous flow around the larvae. Overall, we found that both stages of larvae increased their upward swimming speeds in response to increasing turbulence. However, we found that the early-stage larvae tended to respond to the time-averaged flow whereas the late-stage larvae tended to respond to the instantaneous flow around them. These observations indicate that larvae can integrate flow information over time and that their behavioral responses to turbulence can depend on both their present and past flow environments.

Introduction

The behavior of small plankton in turbulence is of interest across disciplines, from physics to ecology. Turbulence is intermittent, characterized by significant flow variations in time and space. Therefore, plankton in a turbulent environment will experience hydrodynamic fluctuations. Plankton may respond to an individual fluctuation, or they may adjust their behavior in response to the background level of turbulence intensity. The turbulence intensity can be thought of as measurable background noise, whereas fluctuations represent individual signals, and it is not always clear to which the plankton are responding. The time-history of the flow they encounter can be used as an indicator of their local habitat (Fuchs and Gerbi,

2016), e.g., turbulence is typically stronger in the surf zone than in the open ocean. Yet, plankton may also respond to individual hydrodynamic signals, potentially indicative of a nearby predator (e.g., Jakobsen (2001); Kiørboe and Visser (1999)). Turbulence can physically modulate plankton behaviors as well, e.g., by rotating an individual away from its intended heading (Clay and Grünbaum, 2010; Lovecchio et al., 2019; Pujara et al., 2018). Thus, plankton responses to turbulence may be both active and passive and are likely in response to a combination of both their present flow environment and their time-history. While these overlapping signals and responses can not necessarily be separated, together they affect overall behavior.

Many benthic species reproduce through a free-swimming planktonic larval stage. Successful survival, dispersal, and settlement of the larvae depend on both their behavior and their environment (e.g., Cowen and Sponaugle (2009); Koehl and Hadfield (2010); Metaxas (2001)). As ciliated invertebrate larvae are often smaller than 1 mm in diameter (Emlet, 1991), they are typically smaller than the smallest length scales in the flow; therefore, they will experience turbulence largely as a combination of rotation, strain, and acceleration. Isolating these flow signals and the behavioral response they induce in larvae has been a longstanding research goal. For example, Clay and Grünbaum (2010) and McDonald (2012) studied swimming echinoid larvae and embryos respectively, measuring their behavior in vertical shear flow experiments, and showed how shear flow can rotate larvae and alter their upward transport. Fuchs et al. (2018) conducted experiments in separate strain, vorticity, and acceleration dominated flow tanks in order to isolate the different responses of gastropod larvae, finding that larvae of gastropods native to wavy habitats respond more to accelerations than congeneric larvae native to sheltered habitats. These controlled studies provide insight into larval behavior under specific flow signals, yet one must also consider the effects of intermittent forcing inherent to turbulence.

In order to isolate larval behavior in response to intermittent turbulent fluctuations, studies have utilized co-located measurements of the flow and the larvae in turbulence tank experiments (e.g., Fuchs et al. (2015, 2013); Wheeler et al. (2015)). These methods have allowed individual behavioral responses to be isolated, such as the dive response of oyster larvae. This dive response was shown to occur most often after individual larvae experienced a flow acceleration above a certain threshold (Wheeleret al., 2015); but the frequency of the response was also mediated by the ambient turbulence level, and ultimately was observed less frequently under higher turbulence intensity (Wheeler et al., 2013). This suggests that while some larvae can respond to individual turbulent fluctuations, their level of response may be moderated by the background turbulence level. Meanwhile, researchers studying copepods in turbulence found that the copepod jump response was correlated to the background level of turbulence intensity, rather than individual turbulent fluctuations (Michalec et al., 2017). The copepod jump and the dive response of oyster larvae are clear examples of discrete behavioral responses, however other zooplankton may be less obvious in their behavior changes.

While some larvae exhibit active swimming behaviors in response to turbulence, their behavior can also be influenced by passive interactions between hydrodynamic forcing and their morphology. Many motile plankton, including many ciliated larvae, are bottom-heavy with a stable upward swimming posture. Flow rotation (vorticity) can tilt a stable plankter, thus reducing its upward swimming speed, assuming propulsion is kept constant. This effect has been well-described for some phytoplankton (Durham et al.,2009; Kessler, 1985), referred to as gyrotaxis. In turbulence, gyrotactic behavior can create patchy plankton distributions (Durham et al., 2013). In addition, analytical and experimental research have demonstrated that turbulence can alter the upward transport of gyrotactic plankton in a shape-dependent way: namely, spherical plankton show a reduction in transport whereas non-

spherical plankton can show an increase (Gustavsson et al., 2016; Lovecchio et al., 2019). Thus, one must consider the organism's specific morphology.

In this work, we consider the veliger larvae of the gastropod *Crepidula fornicata* (Linnaeus 1758), a widespread suspension-feeder native to eastern North America and invasive throughout Europe (Blanchard, 1997). Like many motile plankton, they are bottom-heavy with a stable upward swimming position in still water, and because they are negatively buoyant, they need to actively swim up to maintain a constant vertical position. However, they can passively sink downward by reducing their swimming propulsion. The Reynolds number of the swimming larvae, characterized by larval size and swimming speed, is of order unity, which means that weak inertia may be important to their dynamics (see discussion in (Klotsa, 2019)). Compared to other plankton studied in turbulence, this Reynolds number is larger than that associated with phytoplankton (Lovecchio et al., 2019), and smaller than that with copepods (Michalec et al., 2015) and ostracods (Sutherland et al., 2011); and thus, larvae of benthic invertebrates represent an intermediate regime of plankton whose behavioral dynamics in turbulence are not well understood.

In order to actively respond to turbulence, larvae need to be able to sense it. *C. fornicata* have different capabilities for sensing their flow environment: they have statocysts that allow them to sense acceleration and rotation, and their ciliatedvelum has the potential to sense strain. Therefore, they can likely sense time-varying turbulent fluctuations, and are an appropriate model organism for this study. In still water, they have demonstrated variable swimming speeds and angular velocities (Chan et al., 2013; DiBenedetto et al., 2021) and while field measurements of vertical distributions have suggested an active upward swimming response to turbulence (Fuchs et al., 2010), direct observations in turbulence have yet to be reported. In addition, unlike the oyster larvae, the *C. fornicata* larvae show no obvious dive response to turbulence, and therefore their behavioral response is likely to be more subtle.

In this study, we sought to further uncover the ways in which larvae respond to turbulence. To measure behavioral response, we conducted experiments with two stages of *C. fornicata* larvae over their development. The study aimed to test the hypothesis that larval behavioral response to turbulence can be characterized solely by considering the instantaneous flow around an individual larva, irrespective of the background level of turbulence, an assumption which has been used to analyze larval behaviorin prior turbulence studies (e.g., Fuchs et al. (2018, 2013)). To test this hypothesis, we varied the background level of turbulence, and considered both time-averaged and instantaneous flow signals along individual larval trajectories. We specifically focused on the larval vertical and horizontal relative velocity response to infer active swimming. Because the size, swimming capabilities, and behavior of *C. fornicata* larvae vary with age (Chan et al., 2013; Penniman et al., 2013), we expected theresponses of the early- and late-stage larvae to vary in magnitude. Furthermore, as larvae develop, they become closer to competence for metamorphosis which may alter their behavior as the larvae seek out suitable locations for settlement.

Materials and Methods

Culturing

Stacks of adult *C. fornicata* were collected by hand from the shallow subtidal zone in Little Harbor, Wareham, MA. The individuals were collected by wading at low tide and were transported to Woods Hole Oceanographic Institution wrapped in *Codium* algae. The adults were cultured in 5 gallon buckets according to Pires (2014). Adults spawned within a few

days in captivity, and larvae were collected within 24 hours by reverse filtration using 150 μm mesh. Cohorts of larvae were collected from two separate adult cohorts. Each cohort was cultured in a clean 5 gallon bucket filled with 10 L of 0.2 μm filtered seawater at a concentration of approximately 250 larvae/L. Aeration was provided by an aquarium bubbler, and the cultures were kept at 20°C. Every other day, the water was changed, the bucket was cleaned, and the larvae were fed. To feed the larvae, live cells from a Tahitian strain of *Isochrysis galbana* were added to the bucket resulting in an average concentration of 10^5 cells/mL, following the protocol of Pires (2014).

The primary difference between the two cohorts of larvae used in the experiments was their age, and will therefore be referred to as early-stage and late-stage larvae. The early-stage cohort hatched July 2nd, 2020 and was cultured for 2 days before running experiments in turbulence. This cohort was pre-competent in their ability to settle. The late-stage cohort hatched June 2nd, 2020 and was cultured for 12 days before running experiments in the turbulence tank. At this stage, the larvae were of the typical age and size when they begin to become competent (Pechenik and Gee, 1993; Pechenik and Heyman, 1987), however competency was not directly tested. A subsample of larval diameters (n=200) was measured directly from the experimental images, with averagediameters of the early-stage larvae measuring $488 \pm 10 \mu$m and the late-stage larvae measuring $758 \pm 9 \mu$m, where uncertainty is denoted with 95% confidence intervals.

Experimental setup

Experiments were conducted in a jet-stirred turbulence tank as depicted in Figure 1(A). The tank was designed and built by students at Grove City College (Grove City, PA) to produce approximately homogeneous and isotropic turbulence in the center of the tank. The design of the tank was inspired by a tank described in Webster et al. (2004), but includes new features that allow for high precision control of jet volume output.

The tank is a 30.5 cm cube with flattened corners, constructed of 0.5 in thick acrylic sheets. Pumps mounted on the eight corners create diffuse pulsing jets of water radiating into the tank. To produce each jet, a sinusoidally driven subwoofer speaker (Tymphany, Peerless, PLS-P830986) actuates a stainless steel bellows (KSM Vacuum Products, Inc., custom design) back and forth in a cylinder (Figure 1B, C). Each cylinder is sealed except for small holes in a printed plastic dome that are confluent with the tank (Figure 1A). As the bellows shortens and extends in the cylinder, water is forced in and out of the holes creating a diffuse jet due to the distribution of holes on the domes and the irreversibility of the high Reynolds number flow regime at the holes. This type of jet is known as a synthetic jet or zero-net-mass-flow jet. An accelerometer (Analog Devices, ADXL377) on a rod connecting the speaker to the bellows is used to determine the stroke length of the bellows in real time, and closed loop control is used to match stroke length for all eight bellows during an experiment, thus resulting in essentially the same volume flow at each dome. This solves the problem faced by Webster et al. (2004), of having to make iterative adjustments to thevoltage sent to the jet pumps based on flow field measurements to achieve isotropic turbulence.

The tank is run with the four pairs of diagonal jet actuators driven 180 degrees out of phase with each other to maintain constant tank volume, preventing pressurization. A virtual signal generator (National Instruments (NI), LabVIEW SignalExpress) and an 8-channel subwoofer power amplifier (Pyle Pro, PET-PYLPT8000CH, 8000 W) drive the speakers. Closed loop control was mediated by a PID control subroutine available in LabVIEW and NI input/output modules (NI-9263 and NI-9201). All jets were operated atthe same pump stroke, or

amplitude, in any given trial. The frequency was kept constant at 30 Hz in all of our experiments, and the pump stroke length was changed to modulate the level of turbulence.

Flow characterization of the tank

The flow in the turbulence tank was initially characterized using particle image velocimetry (PIV). A center-plane of the tank was illuminated with a near-IR pulsed laser (Oxford Firefly FF1000, 300 W), and imaged with a monochromatic CMOS camera (Basler acA2040-90umNIR) equipped with a Nikon micro 105 mm f/2.8 lens. The field of view for the observations was approximately 5.4 cm x 5.4 cm with 377 pixels/cm resolution. The tank was filled with $20 \pm 1^{\circ}$C 0.2μ m filtered seawater, and the entire experiment was conducted within a temperature controlled-environmental chamber set to $20 \pm 1^{\circ}$C. The water was seeded with 11 μm diameter hollow-glass spheres to act as tracer particles; seeding was optimized according to PIV best practices (Raffel et al., 1998). PIV was conducted on image-pairs that were collected at 1 Hz, with a 10 ms delay between frame-pairs, over 17 minutes, over which time the turbulence statistics converged. The PIV was processed using LaVision DaVis software; we used a multi-pass correlation technique with a final resolution of 32x32 pixel boxes with 25% overlap. This resulted in a resolution of 0.06 mm between velocity vectors. The DaVis software processed using the default FFT and sub-pixel fitting with Whittaker reconstruction. The data were post-processed with a median filter.

Kinematic statistics were calculated from the resulting velocity fields, showing approximately isotropic turbulence within a center plane of the tank. Table 1 lists computed quantities for the three turbulence tank settings used in our experiments. The statistical quantities calculated include the root-mean-square of the horizontal and vertical velocity components u_{RMS}, w_{RMS}, the mean of the horizontal and vertical velocity components $\bar{u}, \bar{w}$, turbulence dissipation $varepsilon$, the Kolmogorov length scale $\eta = (\nu^3/\varepsilon)^{1/4}$, and the Reynolds number based on the Taylor microscale $Re_\lambda = u'_{RMS}\lambda/\nu$ (assuming isotropic turbulence), where $\lambda = u'_{RMS}\sqrt{15\nu/\varepsilon}$. As in Webster et al. (2004), we used the approximation $\boldsymbol{u}'_{RMS} = u'_{RMS} = u_{RMS}$ under the assumptions of isotropy and approximately zero mean flow. Dissipation ε was calculated using the 2D velocity gradients by assuming local isotropy, using equation 9 in Xu and Chen (2013). These values are reported for the three turbulence levels considered.

This study utilizes a single-camera PIV and larval tracking system, which can resolve two components of co-located fluid and larval velocity in a two-dimensional (2D) plane. The main behavioral component of interest is the vertical velocity of the larvae, which is accurately measured with a single-camera PIV system. Multi-camera systems, e.g. stereoscopic-PIV, are able to resolve all three components of velocity, including the out-of-plane horizontal velocity, however both single-camera and stereoscopic-PIV are limited by their 2D fields of view. Future studies would benefit from volumetric particle tracking techniques which measure 3D larval trajectories and fluid velocities (e.g. as conducted by Michalec et al. (2017) on copepods).

Data collection for larval experiments

Experiments were conducted separately for the early- and late-stage cohorts in the summer of 2020. All experiments were conducted by a single individual (MHD) due to institutional distancing regulations in place for the COVID-19 pandemic. At the start of the experiment day, approximately 2000 larvae were introduced into the turbulence tank. The turbulence in the tank was then varied, in random order, among the three levels of turbulence in Table 1, (low, medium, high) over 12 individual replicate trials (four trials at each turbulence level). Time between each trial was dependent on the time it took for the tank to re-stabilize at the new turbulence level. For each trial, images were collected continuously for 2-2.5 minutes at a constant turbulence level at a frame rate of 30-40 frames per second, which was adjusted depending on the turbulence level.

After the 12 turbulence trials, the tank's jets were turned off and the larvae were observed in still water, which we refer to as "no forcing". These observations provide a baseline for the larval swimming behavior and ability without turbulence. For the late-stage cohort experiment, another set of turbulence trials was run after the no forcing trials. The length of each experiment was less than 2 hours in total to minimize any changes in larval behavior due to time in the tank.

Due to inherent variation in the setup of the experiment and the short times over which the turbulence trials were run, the computed turbulence quantities show some variation from trial to trial, and overall the early-stage cohort experiment has lower turbulence intensity than the late-stage cohort experiment. However, because the flow is measured simultaneously during the larval experiments, we account for these variations in our analysis.

Data analysis

Measurement of larval swimming speeds in unsteady flow fields necessitates the use of flow subtraction to isolate the motion of the larva relative to that of the flow (Wheeler et al., 2015). The procedure is outlined as follows: we first identify and track the larvae in the field of view; next, we calculate the total larval velocity along each trajectory v_l; we estimate the fluid velocities along each larval trajectory v_f; and we subtract the fluid velocity from the larval velocity to arrive at therelative larval velocity v_r. The fluid velocities and larval velocities were both measured from the same set of images collected during each trial. To start, we identified the larvae as the bright spots in each image by thresholding the image intensity. Next, a predictive tracking algorithm was used to link the centroids of the identified larvae into individual larval trajectories (Kelley and Ouellette, 2011). Along each trajectory, velocities were calculated by cross-correlating image pairs in MATLAB (similar to the methods described by Troutman and Dabiri (2018)). The cross-correlated images around the larvae were square windows with length of 1.5 larval diameters. These larval image pairs were median filtered to remove the tracer particles before a 2D cross correlation was conducted with Gaussian sub-pixel fitting to obtain the displacements between the images.

After calculating the total larval velocities, the fluid velocities were estimated for each larva at each point along its trajectory. The larval trajectories were short, limited by an individual larva's visibility in the camera's depth of field, so no attempt was made to assign velocities to specific larvae. We analyzed the image data using PIV with the same procedure as for the flow characterization study. Veliger larvae affect the flow around them due to their induced feeding and propulsive currents (e.g. see Gallager (1988); Visser (2001)). Therefore, in order to avoid contamination by the larva-induced currents (and contamination of the PIV data by

the larval images), flow vectors close to the larvae were neglected, and the fluid velocity and velocity gradients were interpolated onto the centroid of each larval image using an annulus of PIV velocity data around each larva. The inner annulus radius was 100 pixels (>3 larval diameters) and the outer annulus radius was 200 pixels (>6 larval diameters). The size was optimized based on the PIV vector spacing and the larval wake, including a sensitivity analysis in order to minimize measurement of flow signatures induced by the larvae. The fluid velocity and spatial gradients were fit using a least-squares optimization of a 2D, second-order Taylor series function of the PIV data in the annulus.

The velocity of the larva relative to the fluid, often referred to as the slip velocity, was calculated along each individual trajectory. The horizontal and vertical components of the relative velocity $V_r = (u_r, w_r)$ were calculated by subtracting the interpolated fluid velocity at the larval centroid $V_f = (u_f, w_f)$ from the measured larval velocity in the camera's field of view $V_l = (u_l, w_l)$:

$$u_r = u_l - u_f, \tag{1a}$$

$$w_r = w_l - w_f. \tag{1a}$$

A visualization of the different velocity components is depicted in Figure 2 on a sample experimental image. The relative velocity is not a direct measurement of swimming speed, but rather the resultant velocity of the larva due to swimming propulsion, gravity, and hydrodynamic forces on the larvae such as drag and added mass (Maxey and Riley, 1983) The relative angular velocity $d\phi/dt$ was also measured, where ϕ is the angle of the relative velocity with respect to the positive (upward) vertical axis. We could not measure larval orientation directly with this apparatus, and therefore $d\phi/dt$ here only represents unsteadiness in the direction of the larval velocity relative to the flow.

Because larvae may be able to sense strain, rotation, and acceleration separately, we consider separate characteristics of the flow. To assess strain, we consider turbulent dissipation ε; to assess rotation we consider vorticity ω; andto assess acceleration, we consider the total larval acceleration α. Turbulent dissipation ε is strictly positive. It is calculated using the interpolated spatial gradients and the equation in (Xu and Chen, 2013) which assumes local isotropy. Dissipation is often used to study larval behavior in turbulence (Fuchs et al., 2018, 2010). Vorticity ω in the region of the larva was calculated by integrating the flow velocity around a circle of radius 150 pixels (>4 larval diameters) centered around the larval centroid. The resulting circulation was normalized by the circle area to obtain vorticity. The sign of ω can be both positive and negative, and therefore the absolute value $|\omega|$ is considered in order to characterize vorticity magnitude

The third characteristic considered, α, is simply the acceleration of the larvae in the fixed field of view of the camera, which encompasses the acceleration caused by active swimming and by the passive effect of fluid forcing. It is used here because it is the acceleration experienced by the larval statocysts. Not surprisingly, it also tends to be similar to the acceleration of the flow around the larvae (the average ratio of the flow acceleration to the larval acceleration α_f/α was 1.3 and 1.1 for the early- and late-stage larvae, respectively). The acceleration is calculated along each larval trajectory, and we define α as the absolute value of acceleration $\alpha = \sqrt{du_l/dt^2 + dw_l/dt^2}$.

The three characteristics ε, ω and α are all correlated in our experiments, which is consistent with ideal isotropic turbulence. These correlations can be seen in Figure S1 where bivariate histograms are plotted between $|\omega|$ and ε, and between α and ε. Because these characteristics are strongly correlated, it is not possible to perfectly isolate behavioral responses to each signal. This difficulty has been discussed by Fuchs et al. (2015) and addressed by assessing behavior across different types of flows, such as a straining flow and a rotating flow. In this study, we do not seek to unravel the precise larval response to each individual flow signal, but rather to quantify the overall behavioral response as it relates to the intermittency and intensity of the turbulence. Therefore, we use these turbulence characteristics as indicators of local turbulence intensity.

In order to assess larval behavioral response to the flow, we measured correlations between larval relative velocity and each turbulence characteristic. Trajectory data from all larvae in each treatment were aggregated and analyzed together. To test for any correlation between the flow characteristics $\alpha, |\omega|, \varepsilon$ and relative velocity $w_r, |u_r|$, Spearman's rank correlation coefficients were calculated. Before each correlation test, the relative velocity data were binned by the turbulence characteristic in consideration, where each bin was the average of 100 data points in order to remove noise. Larger bins are used in the figures for clarity. Statistical quantities of the larval kinematics were calculated including RMS and mean values. Bootstrapping was used to calculate 95% confidence intervals on both the reported statistical quantities and the binned data in the plots (Efron and Tibshirani, 1993).

Results

Larval behavior in still water varies over development

We began by characterizing the larval behavior under no forcing for each development stage. Probability density functions (PDFs) were constructed of the relative and angular velocities. The PDFs of horizontal relative velocity u_r, vertical relative velocity w_r, and angular velocity $d\phi/dt$ of the larvae are plotted in Figure 3. Differences in the PDFs between the early- and late-stage larvae can be seen in each case.

With respect to u_r in Figure 3(A), no directional bias is seen for either cohort, as the PDFs are centered around zero. To characterize horizontal swimming, we consider the width of the distributions: the late-stage larvae have a wider distribution of u_r values compared to the early-stage larvae: therefore the late-stage larvae tended to swim faster horizontally than the early-stage larvae. To further quantify this difference, we compare the RMS values of u_r which were found to be 0.058 ± 0.03 and 0.076 ± 0.02 cm s^{-1} for the early- and late-stage cohorts, respectively (1.2 and 1.0 body length s^{-1}) . Overall, we observed an increase in horizontal swimming speeds in still water as the larvae developed.

The PDFs of w_r clearly differ between cohorts in Figure 3(B). The w_r distribution of the early-stage larvae is skewed more positive than that of the late-stage larvae, as most early-stage larvae were observed swimming upward in still water. The average vertical transport of the larvae can be characterized by calculating mean w_r values, which are 0.069 ± 0.002 cm s^{-1} and 0.024 ± 0.003 cm s^{-1} for the early- and late-stage larvae, respectively (1.4 and 0.33

body length s^{-1}) ; in other words, the early-stage larvae on average swam upward at more than twice the rate of the late-stage larvae.

Even though, collectively, the early-stage larvae swam upward at a faster rate than the late-stage larvae, the late-stage larvae exhibited faster maximum swimming speeds and had a larger range of both w_r and u_r values. This shows that the late-stage larvae are able to swim faster than the early-stage larvae individually. This agrees with past observations reported by Chan et al. (2013) which observed an increase in swimming speed over initial larval development of *C. fornicata*. We further characterize swimming ability by comparing maximum upward w_r, which was found to be 0.18 cm s^{-1} and 0.33 cm s^{-1} for the early- and late-stage larvae, respectively (3.7 and 4.3 body length s^{-1}). These values have good agreement with maximum swimming speeds previously reported by Chan et al. (2013) for 2 day and10 day old *C. fornicata* larvae of 0.15 and 0.40 cm s^{-1}, respectively. Finally, the Chan et al. (2013) data show a range of swimming speeds, which is also consistent with our observations.

Angular velocity $d\phi/dt$ provides another metric of behavior in still water. We constructed PDFs of $d\phi/dt$ for each cohort in Figure 3(C). The PDF of the early-stage larvae has more spread than that of the late-stage larvae. We characterize the spread by calculating the RMS of the distributions, which were found to be 1.9 ± 0.1 and 1.5 ± 0.2 deg s^{-1} for the early- and late-stage cohorts, respectively. Therefore, we find that the early-stage larvae exhibited larger angular velocities on average.

Based on these observations, the late-stage larvae have the ability to swim faster upward and horizontally than the early-stage larvae in still water. They also exhibited faster downward velocities, whereas the early-stage larvae were almost exclusively observed swimming upwards. Finally, higher overall angular velocities were observed in the early-stage larvae. Thus, differences in both swimming ability and behavior appear to be present between the early- and late-stage cohorts in still water.

Larval response to instantaneous turbulence characteristics

In this section, we analyze larval behavior as a function only of their immediate flow environment: we consider the flow measured instantaneously at each point in time, and we neglect any effects from the background level of turbulence. To assess behavioral response to the instantaneous turbulence characteristics, we aggregated data from all observed larval trajectories, across all turbulence treatments. The characteristics considered are total larval acceleration α, absolute fluid vorticity $|\omega|$, and turbulent dissipation ε. Larval relative velocity data were binned by each of these and plotted for each cohort in Figure 4.

Both $|u_r|$ and w_r are positively correlated with all flow characteristics considered, and each correlation is statistically significant with Spearman rank test results reported in Table 2. This means that both the horizontal and vertical velocity of all larvae on-average increased with each increasing turbulence characteristic. This suggests the larvae responded to turbulence by increasing their swimming speeds. These correlations do not necessarily indicate direct responses to eachflow characteristic, as all of the flow characteristics are correlated in turbulence (see Figure S1). However, using Spearman rank as an indicator for correlation strength, the strongest correlations for both cohorts are with α, and the weakest correlations are with $|\omega|$.

We can compare the plots for the early- and late-stage larvae to assess variability across development. The $|u_r|$ data collapse for the two cohorts, showing good agreement for all turbulence characteristics (Figure 4(A-C)); this suggests that the horizontal swimming response to turbulence is consistent across larval development. A larger difference between the cohorts was observed in the vertical response (Figure 4(D-F)), where we observe the early-stage larvae increasing their upward velocity in response to all 3 flow characteristics more dramatically than the late-stage larvae. In addition, the w_r values of the early-stage larvae tended to exceed the corresponding late-stage w_r values across all characteristics (Figure 4(D-F)), indicating that the early-stage larvae have a stronger upward swimming response to turbulence than the late-stage larvae when analyzed in this way.

With respect to each turbulence characteristic, the late-stage larvae show more variation in their upward swimming response than the early-stage larvae. For example, a non-monotonic relationship is seen in Figure 4(F) for the late-stage larvae w_r in response to ε, whereas no other response shows this type of curve in Figure 4. In addition, the maximum w_r value for the late-stage larvae in response to ε (Figure 4(F)) is about twice the maximum in value of w_r in response to α and $|\omega|$, indicating that the late-stage larvae do not respond uniformly to all three flow characteristics. In contrast, the early-stage larvae show similar maximum w_r values across flow characteristics. This variability and the generally smaller response observed in the late-stage larvae suggest that as the larvae mature they may become more discerning in how they respond to turbulence.

Larval response to average turbulence level

In the previous section, larval relative velocity was plotted as a function of the instantaneous turbulence characteristics, aggregated across all turbulence experimental trials. In this section, we consider the average background level of turbulence withrespect to the observed larval behaviors. For this analysis, we consider the turbulence tank forcing level (low, medium, high) when analyzing the data.

We first plot larval relative velocities averaged over each experimental trial and treatment (low, medium, high; Table 1) in Figure 5. These velocities characterize the time-averaged larval behavior in turbulence, and are plotted as a function of average ε within that trial. The data reveal similar trends to those observed in the instantaneous data in Figure 4(C). On average, $|u_r|$ increases with ε, following a similar trend for both cohorts. Likewise, w_r increases for the early-stage cohort as a function of ε, whereas the late-stage cohort w_r values show a non-monotonic relationship with ε.

In Figure 6 we plot larval relative velocities against instantaneous larval acceleration α, as in Figure 4(A,C), but in this analysis we have separated the data by turbulence level to explore larval behavioral response to both the instantaneous α and time-averaged flow. We chose α to analyze in this section, as the results in the previous section found it to be the turbulence characteristic with the strongest correlation to larval relative velocity. See the supplementary materials for corresponding plots of relative velocity in response to $|\omega|$ and ε.

Horizontal larval behavior in response to turbulence remained largely unchanged with this new analysis: separating the $|u_r|$ response data by turbulence level yielded similar results to the combined data. For both the early- and late-stage larvae, $|u_r|$ increases with increasing α across all turbulence levels at a similar rate (Figure 6(A,B)), suggesting that instantaneous forcing is most important to horizontal larval behavior and does not change with development.

In the w_r data, however, we see greater differences in the behavior at each turbulence level. The early-stage larvae w_r data clearly segregate by turbulence level, with the highest w_r values seen in the high turbulence level across all α values (Figure 6(C)). In other words, the increase in vertical swimming in response to turbulence is a function of the background turbulence level rather than of the instantaneous forcing. This suggests that the time-history of the larva's flow environment is affecting vertical swimming behavior. In contrast, the late-stage larvae w_r data in Figure 6(D) show minimal segregation by turbulence level except at the lowest values of α. This shows the late-stage larvae have a weaker vertical swimming response to the background turbulence level than the early-stage larvae.

Conclusions and discussion

We tested the hypothesis that larval response to turbulence is due to the instantaneous flow around them. We found that this hypothesis breaks down because organisms can integrate information over time, thus their response can be a function of both the instantaneous forcing and time-averaged quantities. By carefully observing plankton in turbulence, we can begin to parse out the relationship between their behavior and turbulence. Specifically, our observations of the veliger larvae of *C. fornicata* have demonstrated how analyzing larval behaviors with different underlying assumptions can alter our interpretation of their response.

By first observing the larvae in still water, we were able to characterize their swimming abilities in the absence of turbulence. In comparison to the less-developed, early-stage larvae, we observed that the more-developed, late-stage larvae swam faster upward and horizontally, and sank faster downward than the early-stage larvae. The late-stage larvae also exhibited higher variability in their vertical swimming speeds, resulting in a moderate average vertical velocity. Even though the early-stage larvaecould not swim as fast as the late-stage larvae individually, the distribution of their swimming speeds was more positive than that of the late-stage larvae, and thereby had a higher average vertical velocity. These observations indicate that both swimming ability and variability differ between the two cohorts without turbulence. Thus, we expected to see swimming differences between the cohorts with turbulence.

We analyzed our observations of larvae in turbulence multiple ways to elucidate their behavioral responses, starting by assuming that larvae only respond to the instantaneous flow around them. In other words, we assumed larval behavior was only a functionof the flow characteristics in the immediate vicinity of the larva at the time of observation and that the larvae had a short reaction timescale (Pepper et al., 2015). This underlying assumption has been used in other studies to analyze larval behavior in turbulence (e.g., Fuchs et al. (2018, 2013)), and allows us to aggregate observations across all turbulence levels to compare larval behavior against specific turbulence characteristics. We considered total larval acceleration α, absolute vorticity $|\omega|$, and turbulent dissipation ε. For both stages of development, both

components of larval relative velocity, horizontal relative velocity magnitude $|u_r|$ and vertical relative velocity w_r, were positively correlated with all three flow characteristics (see Table 2; Figure 4). This result suggests that larvae increase their relative velocity, and therefore their swimming speed, as the flow around them becomes generally more turbulent. Finally, of the three turbulence characteristics, α had the strongest correlations with relative velocity, and $|\omega|$ had the lowest. This suggests that the larvae activelysense and respond to flow accelerations in turbulence with their statocysts, a behavior which has previously been observed in larval mud snails *Tritia trivittata* (Fuchs et al., 2018).

Next, we assumed that the larval behavioral response might be mediated by the time-averaged turbulence level, and indeed we found larval behavior to be more complex than revealed considering only the previous assumption. Within this framework, we segregated the observations by the background turbulence level, and conducted a similar analysis as before, but now with separate curves for each turbulence level (see Figure 6), considering only α. If behavior was independent of the time-averaged turbulence and only a function of the instantaneous flow within the larvaâ€™s immediate vicinity, then the curves should collapse. This collapse across turbulence levels was seen in $|u_r|$, for both cohorts (Figures 6(A,B)), suggesting that horizontal behavior of the larvae is mediated significantly by the instantaneous flow and is relatively independent of the time-averaged flow. Therefore, changes to larval horizontal behavior maynot be reflective of their time-history but rather of their immediate surroundings.

In contrast with the horizontal behavior, the larval vertical swimming behavior has a strong response to the average turbulence level. This relationship is seen in Figure 6(C) which shows a clear segregation in w_r by turbulence level for the early-stage larvae, suggesting that the larval vertical swimming behavior was strongly mediated by the time-averaged flow rather than the instantaneous forcing. The w_r data of the late-stage larvae collapse at higher levels of α (Figure 6D), but show segregation at lower values. This partial collapse suggests a complex response to turbulence that is somewhat dependent on their time-history. If a larva's response to the turbulent flow characteristics was solely a function of the flow in their immediate surroundings, there would be no difference in the data in Figure 6 with respect to each turbulence level. The presence of separation in the data proves our hypothesis wrong and demonstrates that larval behavior can be both a function of the fluctuating turbulent signal and the background level of turbulent noise. Future studies of larval behavior in turbulence should make sure to account for these potential interactions.

Larval swimming behavior is inherently anisotropic; upward swimming is needed to oppose gravitational settling, and environmental variables such as light, food, and ocean currents are often vertically stratified in the ocean. Therefore, like most larvae,*C. fornicata* larvae tend to swim faster in the vertical direction than in the horizontal (DiBenedetto et al., 2021). In this study, we also found anisotropic behavioral responses to turbulence. The horizontal response to increase $|u_r|$ with increasing instantaneous turbulence characteristics was similar for both the early- and late-stage larvae, with no strong variation with background turbulence level. The vertical behavior showed a much stronger response to the background level, but also showed an increase in w_r with increasing background turbulence. This contrast suggests that the larvae do not necessarily increase their vertical and horizontal swimming behaviors in tandem in response to turbulence, but rather adjust each one independently.

As turbulence intensity increases, a passive larva will be increasingly tilted by the flow's vorticity. Larval tilting alone would reduce upward swimming speed in the absence of increased propulsion (e.g. see Wheeler et al. (2016)). In response to increasing turbulence (and therefore vorticity), we in fact observed an increase in upward swimming, implying the larvae actively respond to turbulence by increasing their upward swimming speed. However, we also observed an increase in horizontal relative velocity under turbulence, a response which could be explained by an increase in larval tilting. Because the upward swimming increased with respect to turbulent forcing, the larvae must have increased their swimming speed, indicating an active response. Larval swimming speed cannot increase with increasing turbulence intensity indefinitely, and at a higher level of turbulence intensity, the vorticity will tilt the larvae such that they can no longer swim upwards, however this threshold must occur at turbulence levels higher than we are able to produce in our facility.

The two stages of *C. fornicata* larvae observed likely varied in their response to turbulence because of their differing levels of development. The early-stage larvae were pre-competent and not yet ready to settle; their tendency to swim upward would keep them higher in the water column and promote dispersal. In addition, their increase in upward swimming speed would help counteract the effects of turbulence mixing them downward. The late-stage larvae were approaching competency, and therefore the variability seen in their swimming speed and direction could indicate exploratory behavior looking for suitable locations for settlement. Their response to turbulence was moderate compared to that of the early-stage larvae, and therefore they would be moreeasily mixed downward by turbulence; downward mixing by turbulence may be beneficial to the late-stage larvae because they are closer to competency and will have to ultimately sink downward to settle.

The effects of larval size may also influence larval response to turbulence. In this study, both larval cohorts were on-average smaller than the smallest turbulence length scale, the Kolomogorov length scale η, for most cases (see Table 1), however the late-stage larvae were approximately the size of η at the high turbulence level. When larvae are approximately the same size or larger than η, the assumption that the flow around them can be approximated linearly breaks down, and the larvae can feel multiple scales of the flow at once (see Wheeler et al. (2019)). This effect may alter a larva's ability to interpret the instantaneous flow around them, and may partly explain why the larger larvae were less responsive to the turbulence than the smaller larvae. However, because there was no strong change in flow response relative to the low and medium turbulence level where the old larvae were much smaller than η, the difference in larval size between cohorts does not likely explain their observed differential response in these experiments.

While our experiments provide the first direct measurements of *C. fornicata* larval response to turbulence, indirect measurements have been reported during a field campaign (Fuchs et al., 2010). In a well-mixed tidal inlet, observations of larval concentrations, turbulence conditions, and temperature were collected, and using an advection-diffusion model, the authors inferred larval vertical swimming speeds as a function of turbulent dissipation. Fuchs et al. (2010) found that *Crepidula spp.* larvae sank in weak turbulence and swam upward in strong turbulence. They further deduced that small larvae were more sensitive to turbulence than the large larvae; in other words, the small larvae started swimming upwards at lower levels of turbulence.

Their results are well-aligned with our observations that both cohorts show an increase in upward swimming in response to turbulence, and that the early-stage larvae are more responsive to the turbulence. This agreement lends credence to the assumption that the behaviors observed in our laboratory setting are representative of behaviors in the field.

Acknowledgements

We would like to thank the students of the senior design teams and the Anderson Lab in the Department of Mechanical Engineering at Grove City College who designed, built, and improved the turbulence tank under the guidance of EJA during 2012-19. We thank the Grove City College Department of Mechanical Engineering for funding the design and construction of the tank. We also thank Don Webster for communicating with the 2012-13 design team regarding the tank used by Webster et al. (2004).

Competing interests

The authors declare no competing interests.

Contribution

MHD designed the experiments, collected the data, analyzed the data, and drafted the manuscript. KRH and LSM assisted with experimental design and data collection. EJA designed and led the construction of the turbulence tank. AP assisted with organism collection and culturing. All authors critically revised the manuscript, gave final approval for publication and agree to be held accountable for the work performed therein.

Funding

MHD acknowledges funding from the Woods Hole Oceanographic Institution Postdoctoral Scholarship. EJA was supported by grants from the Swezey and the Jewell, Moore, and MacKenzie Funds of Grove City College. LSM was supported by NSF grant OCE-1947735 and WHOI internal funds.

Data availability

Data can be found online at https://figshare.com/s/d2adfbdf1cbc07bf09f7

References

Blanchard, M. (1997). Spread of the slipper limpet crepidula fornicata (l. 1758) in europe. current state dans consequences. *Scientia marina* **61**, 109–118.

Chan, K. Y. K., Jiang, H. and Padilla, D. K. (2013). Swimming speed of larval snail does not correlate with size and ciliary beat frequency. *PLoS ONE* **8**, 6–13. DOI: 10.1371/journal.pone.0082764.

Clay, T. W. and Grünbaum, D. (2010). Morphology-flow interactions lead to stage-selective vertical transport of larval sand dollars in shear flow. *Journal of Experimental Biology* **213**, 1281–1292. DOI: 10.1242/jeb.037200.

Cowen, R. K. and Sponaugle, S. (2009). Larval Dispersal and Marine Population Connectivity. *Annual Review of Marine Science* **1**, 443–466. DOI: 10.1146/annurev.marine.010908.163757.

DiBenedetto, M. H., Meyer-Kaiser, K. S., Torjman, B., Wheeler, J. D. and Mullineaux, L. S. (2021). Departures from isotropy: the kinematics of a larval snail in response to food. *Journal of Experimental Biology* **224**. DOI: 10.1242/jeb.239178.

Durham, W. M., Climent, E., Barry, M., De Lillo, F., Boffetta, G., Cencini, M. and Stocker, R. (2013). Turbulence drives microscale patches of motile phytoplankton. *Nature communications* **4**, 2148. DOI: 10.1038/ncomms3148.

Durham, W. M., Kessler, J. O. and Stocker, R. (2009). Disruption of vertical motility by shear triggers formation of thin phytoplankton layers. *science* **323**, 1067–1070.

Efron, B. and Tibshirani, R. J. (1993). *An introduction to the bootstrap*. Chapman and Hall.

Emlet, R. B. (1991). Functional constraints on the evolution of larval forms of marine invertebrates: experimental and comparative evidence. *American Zoologist* **31**, 707–725.

Fuchs, H. L. and Gerbi, G. P. (2016). Seascape-level variation in turbulence-and wave-generated hydrodynamic signals experienced by plankton. *Progress in Oceanography* **141**, 109–129.

Fuchs, H. L., Gerbi, G. P., Hunter, E. J. and Christman, A. J. (2018). Waves cue distinct behaviors and differentiate transport of congeneric snail larvae from sheltered versus wavy habitats. *Proceedings of the National Academy of Sciences* **115**, E7532–E7540. DOI: 10.1073/pnas.1804558115.

Fuchs, H. L., Gerbi, G. P., Hunter, E. J., Christman, A. J. and Diez, F. J. (2015). Hydrodynamic sensing and behavior by oyster larvae in turbulence and waves. *Journal of Experimental Biology* **218**, 1419–1432. DOI: 10.1242/jeb.118562.

Fuchs, H. L., Hunter, E. J., Schmitt, E. L. and Guazzo, R. A. (2013). Active downward propulsion by oyster larvae in turbulence. *Journal of Experimental Biology* **216**, 1458–1469. DOI: 10.1242/jeb.079855.

Fuchs, H. L., Solow, A. R. and Mullineaux, L. S. (2010). Larval responses to turbulence and temperature in a tidal inlet: Habitat selection by dispersing gastropods? *Journal of Marine Research* **68**, 153–188. DOI: 10.1357/002224010793079013.

Gallager, S. M. (1988). Visual observations of particle manipulation during feeding in larvae of a bivalve mollusc. *Bulletin of marine Science* **43**, 344–365.

Gustavsson, K., Berglund, F., Jonsson, P. R. and Mehlig, B. (2016). Preferential Sampling and Small-Scale Clustering of Gyrotactic Microswimmers in Turbulence. *Physical Review Letters* **116**, 1–6. DOI: 10.1103/PhysRevLett.116.108104.

Jakobsen, H. H. (2001). Escape response of planktonic protists to fluid mechanical signals. *Marine Ecology Progress Series* **214**, 67–78.

Kelley, D. H. and Ouellette, N. T. (2011). Using particle tracking to measure flow instabilities in an undergraduate laboratory experiment. *American Journal of Physics* **79**, 267–273. DOI: 10.1119/1.3536647.

Kessler, J. O. (1985). Hydrodynamic focusing of motile algal cells. *Nature* **313**, 218–220.

Kiørboe, T. and Visser, A. W. (1999). Predator and prey perception in copepods due to hydromechanical signals. *Marine Ecology Progress Series* **179**, 81–95.

Klotsa, D. (2019). As Above, So Below, and also in Between: Mesoscale active matter in fluids. *Soft Matter* **15**. DOI: 10.1039/c9sm01019j.

Koehl, M. A. R. and Hadfield, M. G. (2010). Hydrodynamics of larval settlement from a larva's point of view. *Integrative and Comparative Biology* **50**, 539–551. DOI: 10.1093/icb/icq101.

Lovecchio, S., Climent, E., Stocker, R. and Durham, W. M. (2019). Chain formation can enhance the vertical migration of phytoplankton through turbulence. *Science Advances* **5**. DOI: 10.1126/sciadv.aaw7879.

Maxey, M. R. and Riley, J. J. (1983). Equation of motion for a small rigid sphere in a nonuniform flow. *Physics of Fluids* **26**, 883. DOI: 10.1063/1.864230.

McDonald, K. A. (2012). Earliest ciliary swimming effects vertical transport of planktonic embryos in turbulence and shear flow. *Journal of Experimental Biology* **215**, 141–151. DOI: 10.1242/jeb.060541.

Metaxas, A. (2001). Behaviour in flow: Perspectives on the distribution and dispersion of meroplanktonic larvae in the water column. *Canadian Journal of Fisheries and Aquatic Sciences* **58**, 86–98. DOI: 10.1139/f00-159.

Michalec, F.-G., Fouxon, I., Souissi, S. and Holzner, M. (2017). Zooplankton can actively adjust their motility to turbulent flow. *Proceedings of the National Academy of Sciences* **114**, E11199–E11207.

Michalec, F. G., Souissi, S. and Holzner, M. (2015). Turbulence triggers vigorous swimming but hinders motion strategy in planktonic copepods. *Journal of the Royal Society Interface* **12**. DOI: 10.1098/rsif.2015.0158.

Pechenik, J. A. and Gee, C. C. (1993). Onset of metamorphic competence in larvae of the gastropod crepidula fomicata (l.), judged by a natural and an artificial cue. *Journal of Experimental Marine Biology and Ecology* **167**, 59–72.

Pechenik, J. A. and Heyman, W. D. (1987). Using kcl to determine size at competence for larvae of the marine gastropod crepidula fornicata (l.). *Journal of Experimental Marine Biology and Ecology* **112**, 27–38.

Penniman, J. R., Doll, M. K. and Pires, A. (2013). Neural correlates of settlement in veliger larvae of the gastropod, c repidula fornicata. *Invertebrate Biology* **132**, 14–26.

Pepper, R. E., Jaffe, J. S., Variano, E. and Koehl, M. A. R. (2015). Zooplankton in flowing water near benthic communities encounter rapidly fluctuating velocity gradients and accelerations. *Marine Biology* **162**, 1939–1954. DOI: 10.1007/s00227-015-2713-x.

Pires, A. (2014). Artificial seawater culture of the gastropod *crepidula fornicata* for studies of larval settlement and metamorphosis. In *Developmental Biology of the Sea Urchin and Other Marine Invertebrates*. Springer, pages 35–44.

Pujara, N., Koehl, M. A. R. and Variano, E. A. (2018). Rotations and accumulation of ellipsoidal microswimmers in isotropic turbulence. *Journal of Fluid Mechanics* **838**, 356–368. DOI: 10.1017/jfm.2017.912.

Raffel, M., Willert, C. E., Kompenhans, J. et al. (1998). *Particle image velocimetry: a practical guide*, volume 2. Springer.

Sutherland, K. R., Dabiri, J. O. and Koehl, M. A. R. (2011). Simultaneous field measurements of ostracod swimming behavior and background flow. *Limnology and Oceanography: Fluids and Environments* **1**, 135–146. DOI: 10.1215/21573698-1472410.

Troutman, V. A. and Dabiri, J. O. (2018). Single-camera three-dimensional tracking of natural particulate and zooplankton. *Measurement Science and Technology* **29**, 075401.

Visser, A. W. (2001). Hydromechanical signals in the plankton. *Marine Ecology Progress Series* **222**, 1–24.

Webster, D. R., Brathwaite, A. and Yen, J. (2004). A novel laboratory apparatus for simulating isotropic oceanic turbulence at low reynolds number. *Limnology and Oceanography: Methods* **2**, 1–12.

Wheeler, J. D., Chan, K. Y. K., Anderson, E. J. and Mullineaux, L. S. (2016). Ontogenetic changes in larval swimming and orientation of pre-competent sea urchin Arbacia punctulata in turbulence. *The Journal of Experimental Biology* **219**, 1303–1310. DOI: 10.1242/jeb.129502.

Wheeler, J. D., Helfrich, K. R., Anderson, E. J., McGann, B., Staats, P., Wargula, A. E., Wilt, K. and Mullineaux, L. S. (2013). Upward swimming of competent oyster larvae Crassostrea virginica persists in highly turbulent flow as detected by PIV flow subtraction. *Marine Ecology Progress Series* **488**, 171–185. DOI: 10.3354/meps10382.

Wheeler, J. D., Helfrich, K. R., Anderson, E. J. and Mullineaux, L. S. (2015). Isolating the hydrodynamic triggers of the dive response in eastern oyster larvae. *Limnology and Oceanography* **60**, 1332–1343. DOI: 10.1002/lno.10098.

Wheeler, J. D., Secchi, E., Rusconi, R. and Stocker, R. (2019). Not Just Going with the Flow: The Effects of Fluid Flow on Bacteria and Plankton. *Annual Review of Cell and Developmental Biology* **35**, 213–237. DOI: 10.1146/annurev-cellbio-100818-125119.

Xu, D. and Chen, J. (2013). Accurate estimate of turbulent dissipation rate using PIV data. *Experimental Thermal and Fluid Science* **44**, 662–672. DOI: 10.1016/j.expthermflusci.2012.09.006.

Figures

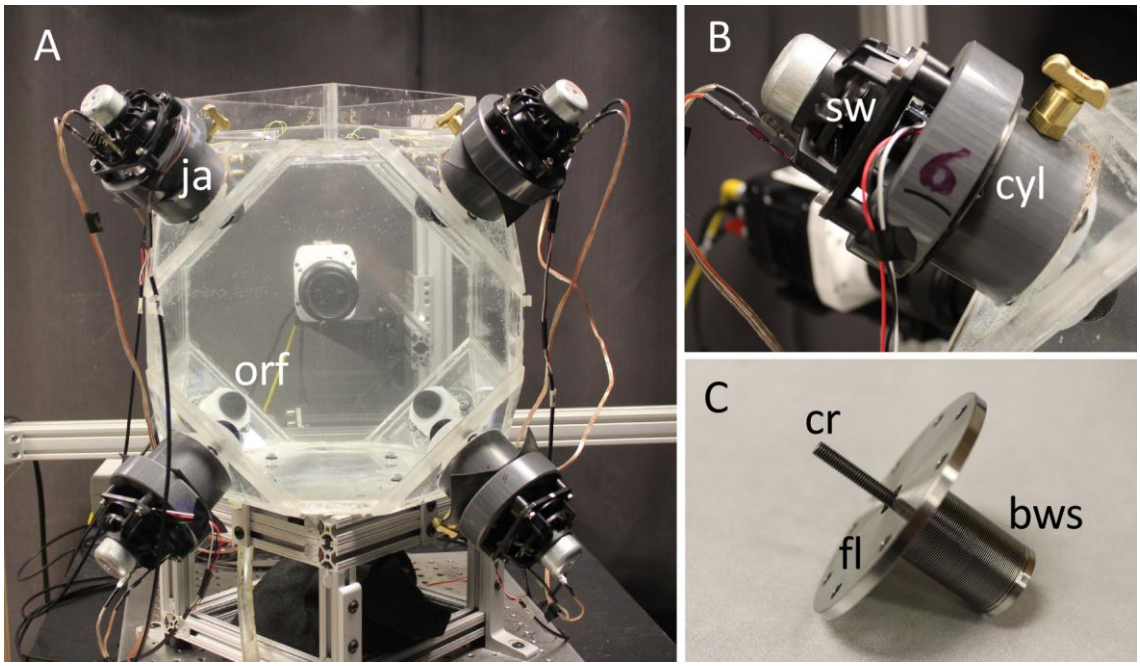

Figure 1. Images of the turbulence tank (A), a jet actuator (B) and the bellows assembly that displaces fluid in the jet actuator cylinders (C). In the whole tank view, four of the eight jet actuators (ja) and some of the black domed orifices (orf) of the tank are visible. The close-up of the jet actuator shows the subwoofer speaker (sw), then wires leading to the accelerometer on the rod connecting the speaker to the bellows inside the cylinder (cyl). The bellows (bws) assembly shows the connecting rod (cr) and the flange (fl), which is the lid of the fluid cylinder. The flange and cylinder are sealed with a rubber gasket (not shown) and the cylinder is connected to the tank wall with glue and fasteners.

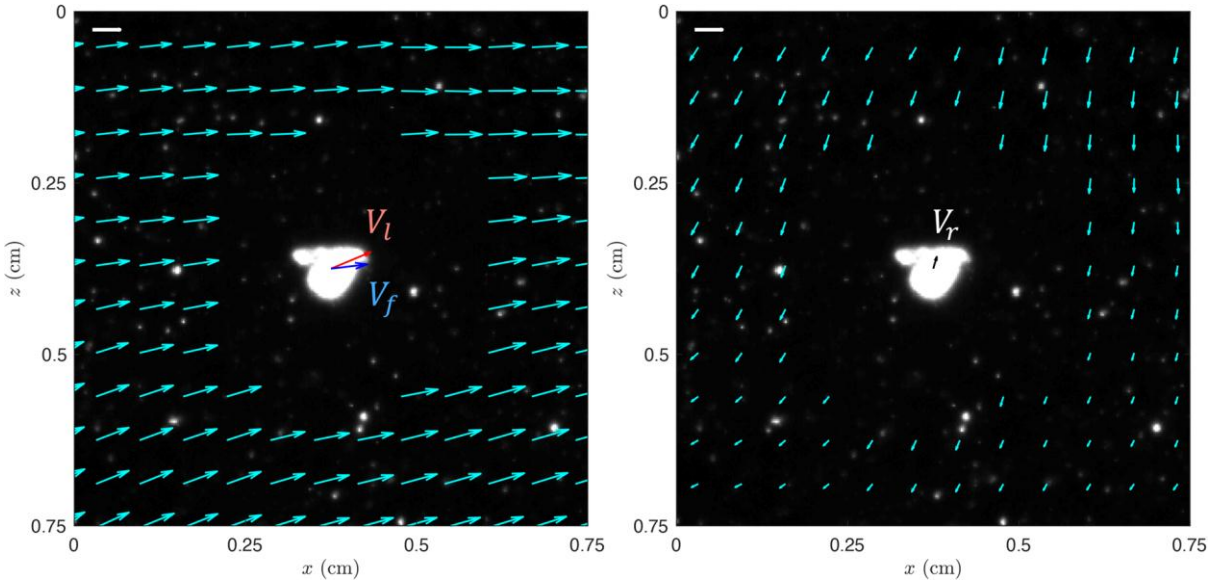

Figure 2. Larval and fluid velocity measurements. A snapshot of a late-stage larva in the medium level of turbulence is shown with different velocity vectors. The image is a small portion of the total field of view, centered around the larva. (Left) Larval velocity $\boldsymbol{v}_l = (u_l, w_l)$ and interpolated fluid velocity at the larva $\boldsymbol{v}_f = (u_f, w_f)$ are plotted with background vector field showing measured fluid velocity. (Right) Relative larval velocity $V_r = (u_r, w_r)$ is plotted with background vector field showing relative fluid velocity ($V_f - V_l$). Scale bar drawn in the top left corner of each image represents 5 mm s^{-1}.

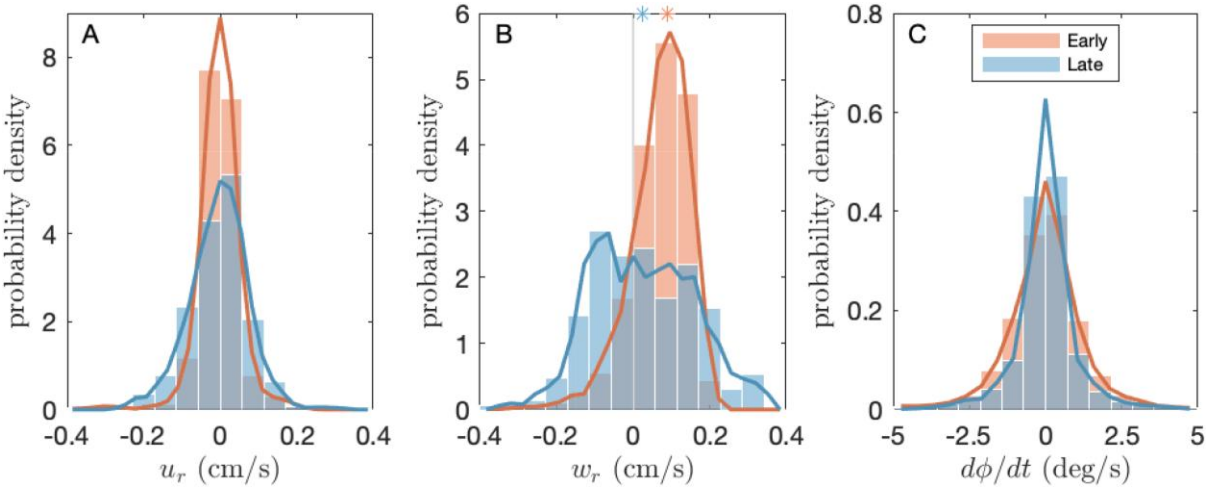

Figure 3. Larval kinematics in still water for early- and late-stage larvae. (A) Horizontal relative velocity u_r probability density functions, and (B) vertical relative velocity w_r probability density functions for both larval cohorts. Median values of w_r for each data set marked with *. (C) Angular velocity $d\phi/dt$ probability density functions for both cohorts.

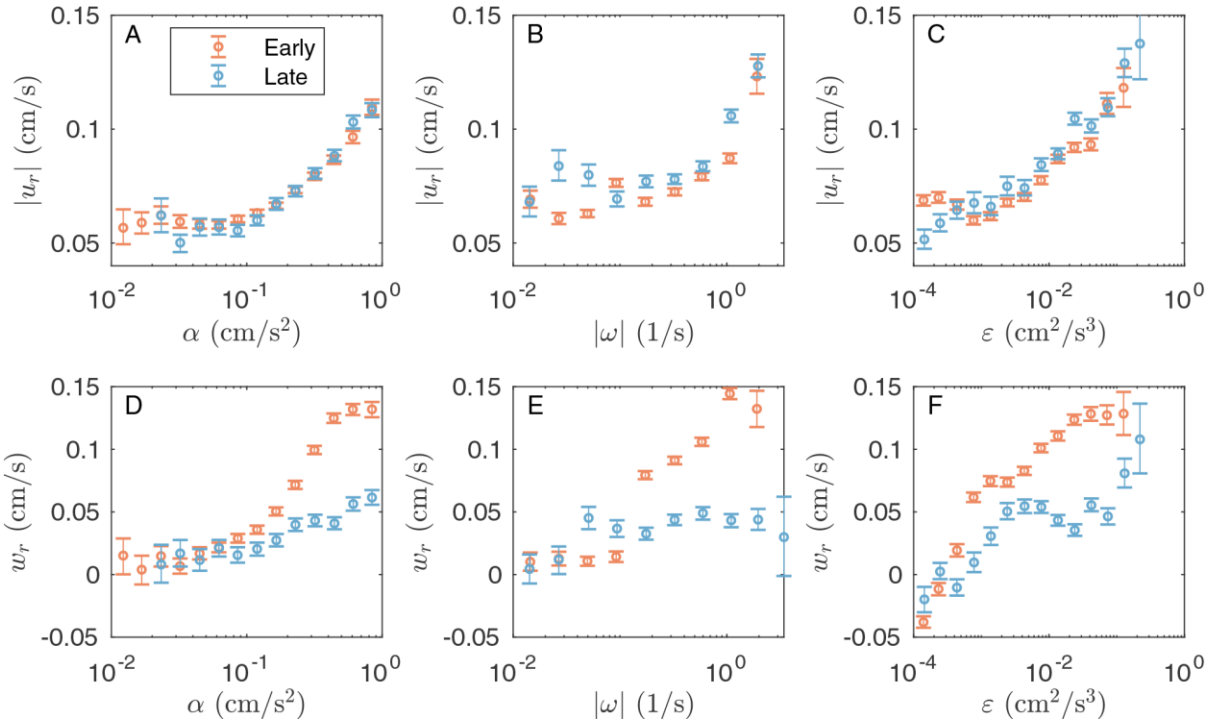

Figure 4. Relative velocity of larvae in turbulence, associated with three different turbulence characteristics. Horizontal relative velocity $|u_r|$ shown in (A-C) and vertical relative velocity w_r shown in (D-F), as a function of larval acceleration α (A,D), flow vorticity $|\omega|$ (B,E), and turbulent dissipation ε (C,F). Absolute values are used for horizontal relative velocity and flow vorticity to display magnitude. The data are binned, and the error bars denote 95% confidence intervals determined by bootstrapping the data in each bin. Corresponding Spearman rank correlation tests for each relationship have positive correlation with statistical significance; see Table 2.

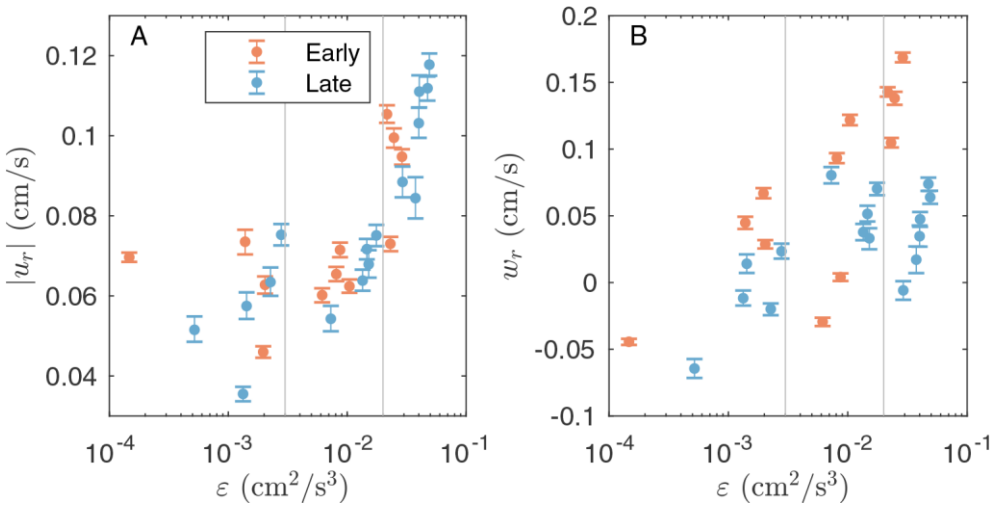

Figure 5. Relative larval velocities averaged over each trial as a function of turbulent dissipation. (A) Average horizontal relative velocity magnitude $|u_r|$, and (B) average vertical relative velocity w_r are plotted for both cohorts with error bars showing 95% confidence intervals determined with bootstrapping. The vertical lines denote the rough boundaries of dissipation rates generated at the low, medium, and high turbulence tank levels.

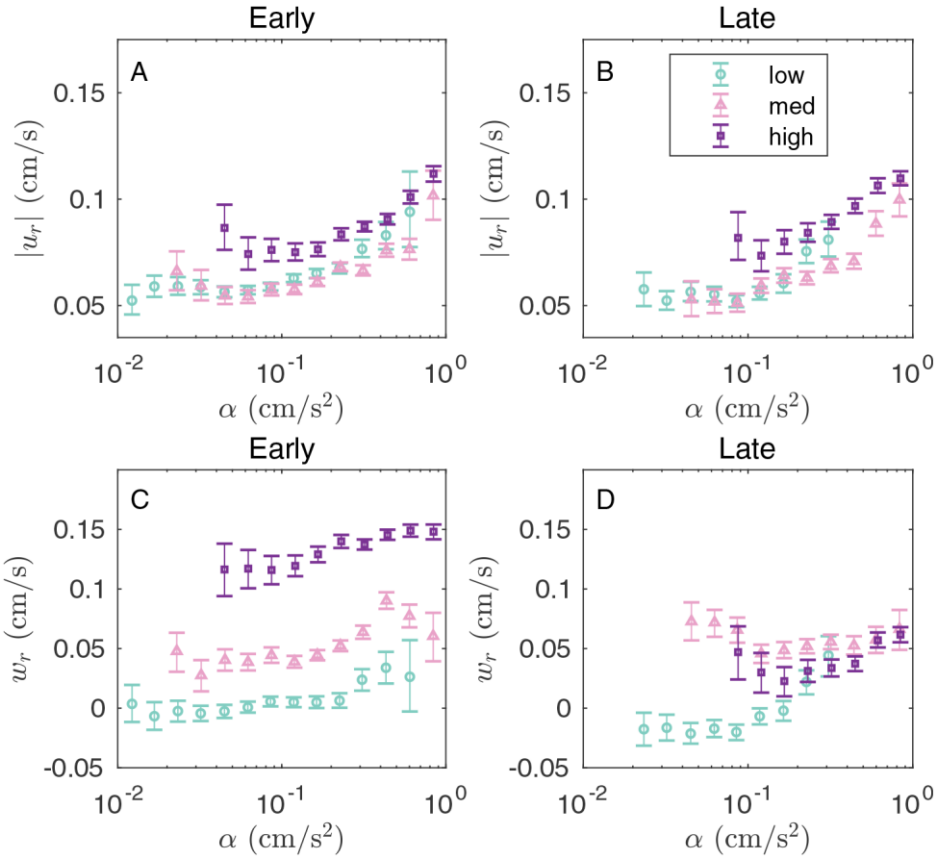

Figure 6. Relative velocities as a function of instantaneous larval acceleration α segregated by turbulence level. Early-stage larvae data shown in plots (A,C) and late-stage data shown in plots (B,D). Horizontal relative velocity magnitude $|u_r|$ is plotted in (A,B), and vertical relative velocity w_r is plotted in (C,D). The turbulence levels correspond to low, medium, and high forcing, and the data are binned with error bars representing 95% confidence intervals for the mean of each bin.

Table 1. Summary of statistics for each turbulence level under initial characterization.

Turbulence level	Low	Medium	High
u_{RMS} (cm s^{-1})	0.18	0.35	0.50
w_{RMS} (cm s^{-1})	0.17	0.31	0.46
$\overline{u}$ (cm s^{-1})	-0.056	-0.034	-0.037
$\overline{w}$ (cm s^{-1})	-0.032	0.22	-0.065
ε (cm^2 s^{-3})	0.0025	0.0081	0.022
η (cm)	0.14	0.11	0.082
λ (cm)	1.45	1.50	1.30
Re_λ	27	52	65

Table 2. Spearman rank, ρ_s, for each flow characteristic correlated against horizontal relative velocity magnitude and vertical relative velocity as plotted in Figure 4. All p-values < 0.001.

		α	$\lvert\omega\rvert$	ε
Early-stage	$\lvert u_r \rvert$	0.90	0.55	0.76
	w_r	0.94	0.86	0.90
Late-stage	$\lvert u_r \rvert$	0.94	0.70	0.84
	w_r	0.69	0.25	0.32

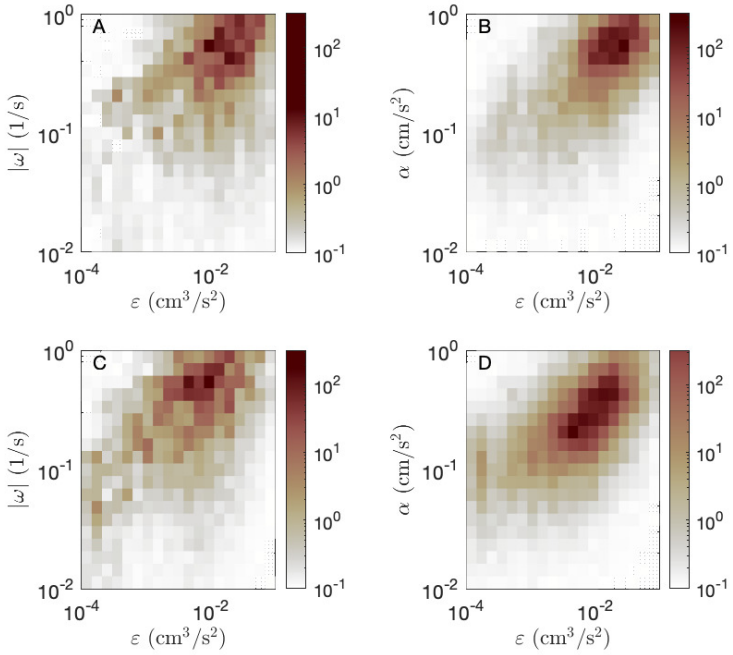

Fig. S1. Bivariate histograms of instantaneous absolute vorticity and absolute larval acceleration against instantaneous dissipation for all turbulence experiments. (A,B) Data from early-stage larvae experiments and (C,D) data from late-stage larvae experiments shown separately. The colorbar refers to number of observations.

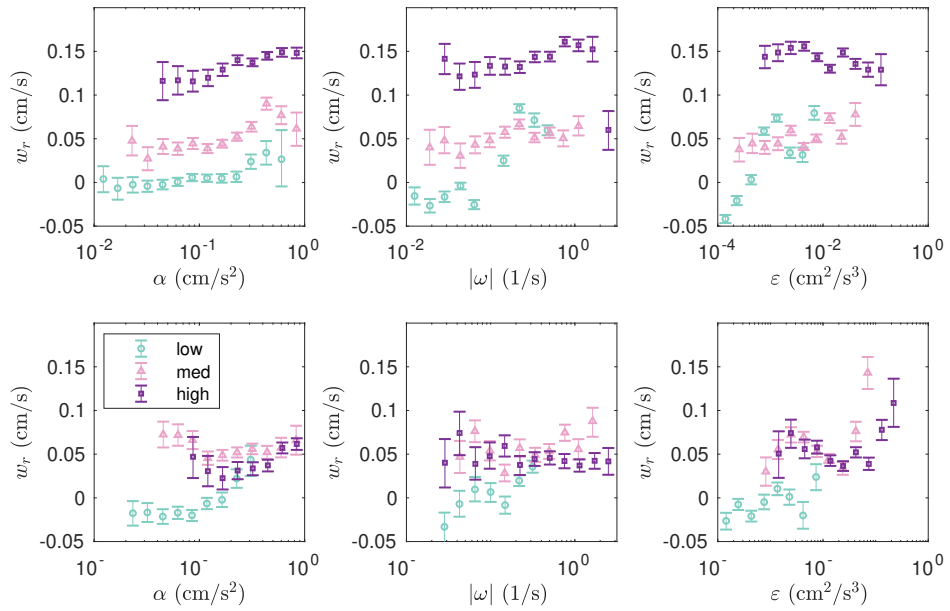

Fig. S2. Vertical w_r relative velocity of larvae in turbulence as a function of turbulence characteristics. Larval acceleration α, flow vorticity ω, and turbulent dissipation ε are plotted. Early-stage larvae data is plotted in the top row and late-stage larvae data is plotted in the bottom row. The error bars denote 95% confidence intervals determined by bootstrapping the data in each bin.

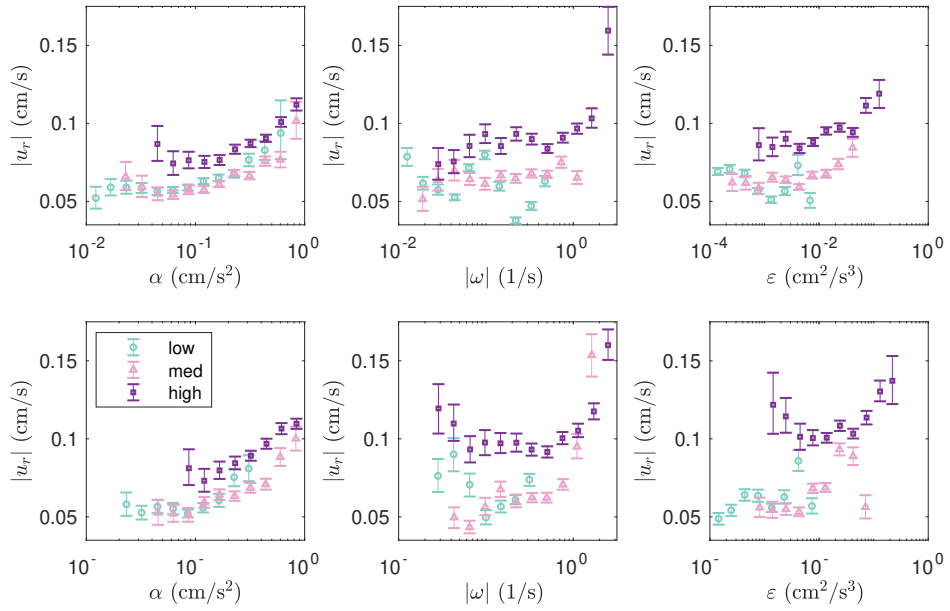

Fig. S3. Absolute horizontal relative velocity $|u_r|$ as a function of turbulence characteristics. Larval acceleration α, flow vorticity ω, and turbulent dissipation ε are plotted. Early-stage larvae data is plotted in the top row and late-stage larvae data is plotted in the bottom row. The error bars denote 95% confidence intervals determined by bootstrapping the data in each bin.

Datast S1.

Click here to download Dataset 1